BBAA VI International Colloquium on:
Bluff Bodies Aerodynamics & Applications
Milano, Italy, July, 20-24 2008

# WIND TUNNEL AND CFD MODELLING OF PRESSURES ON DOWNWIND SAILS

**Peter Richards[*] and William Lasher[†]**

[*]Department of Mechanical Engineering
University of Auckland, Private Bag 92019, Auckland, New Zealand
e-mail: pj.richards@auckland.ac.nz,

[†] School of Engineering
Penn State Erie, The Behrend College, Erie, PA, USA
e-mail: wcl2@psu.edu

**Keywords:** Sails, Spinnaker and Mainsail, Surface Pressures.

**Abstract** *Wind tunnel testing of pressure tapped fibreglass downwind sails and CFD modelling are used to investigate the flow around and the interactions between 1/25th scale IACC sails. It is shown that when trimmed for maximum thrust, the mainsail has a small beneficial effect on the flow around the spinnaker. However, the spinnaker has a small adverse effect on the mainsail. These interaction effects are shown to be a mixture of changes to the local flow angles and the overlapping of the pressure fields around each sail.*

## 1 INTRODUCTION

In order to gain further understanding of downwind sails, pressure tapped fibreglass models have been tested in the University of Auckland Twisted Flow Wind Tunnel (Fig. (1a)). Complimentary computational modelling (Fig. (1b)) has also been carried out using the Fluent CFD code. This study is an extension of work previously carried out by the authors [1].

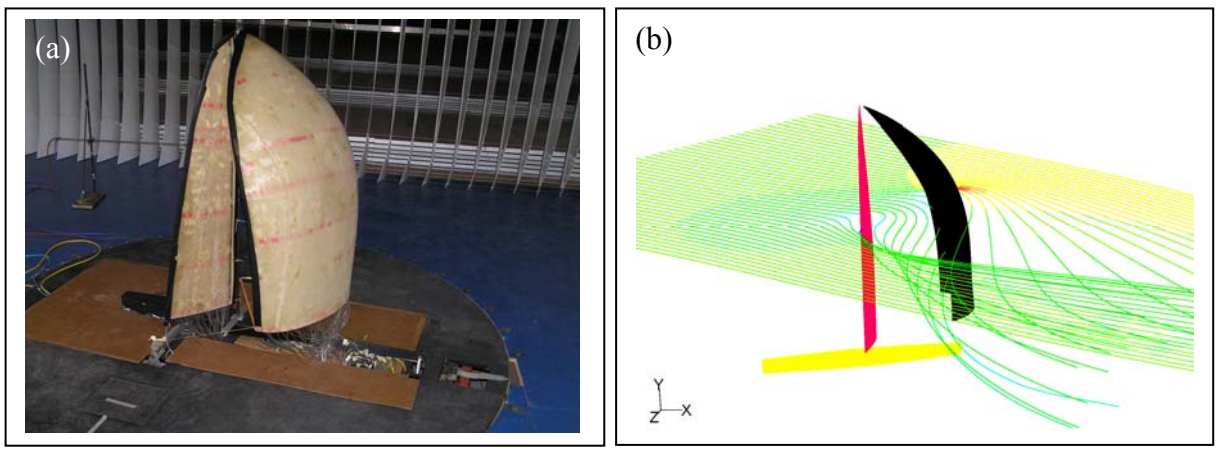


Figure 1: (a) The wind-tunnel model and (b) An isometric view of the CFD model

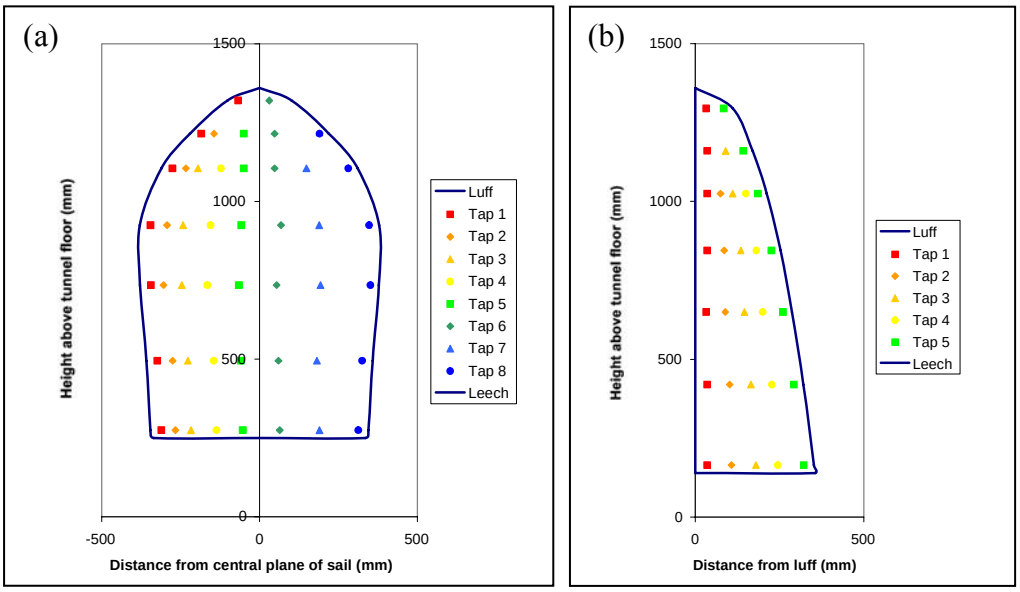


Figure 2: Tap locations on the wind tunnel sails (a) Spinnaker and (b) Mainsail

## 2 EXPERIMENTAL AND CFD METHODS

1/25$^{th}$ scale models of generic International America's Cup Class (IACC) main and symmetric spinnaker sails have been modelled in the wind tunnel by constructing these from two thin fibreglass layers. The spinnaker had 47 pressure taps on each surface and the mainsail 30 taps on each surface, which were arranged as seven rows of taps across each sail, as illustrated in Fig. (2). In recent years America's Cup races have consisted of a simple series of windward and leeward legs, where the marks are placed such that the wind flows directly from the top mark to the bottom mark. This means that the sailors choose a direction which maximises the Velocity Made Good (VMG), which is the component of the boat velocity in the wind direction. When sailing into the wind this is achieved by sailing with a true wind angle of about 35°. When sailing downwind it is possible to head directly downwind, but in such cases the apparent wind, which is the wind speed minus the boat speed, is weak and so the driving force is low. In moderate winds it is better to sail at a true wind angle around 150-160° where the vector sum of the velocities creates a significantly larger apparent wind speed and hence thrust. The target velocity and twist profiles used in this study were based on an IACC yacht sailing at a true wind angle of 160° at a speed of 10.5 kts (5.25 m/s) in a true wind of 14 kts (7 m/s) at a reference height of 10m, which corresponds to a reference apparent wind angle of 120°. Fig. (3) shows a speed polar for a generic IACC yacht. In this figure the true wind is vertically down the page and the radial position of the various lines shows the speed that can be achieved when sailing in a particular direction with each true wind speed. The superimposed vectors represent the chosen reference condition where with 7 m/s of true wind (at the reference height of 10m) the downwind VMG is maximised (lowest point on the curve) with a true wind angle of 160°. The polar shows that under these conditions the boat speed is 5.25 m/s along the 160° radial. By adding the scaled true wind vector, the apparent wind vector can be constructed as

$$\mathbf{V}_A = \mathbf{V}_T - \mathbf{V}_B \qquad (1)$$

which is a vector with magnitude 2.75 m/s along the 40° radial, indicating an apparent wind direction of 120° relative to the direction the boat is sailing.

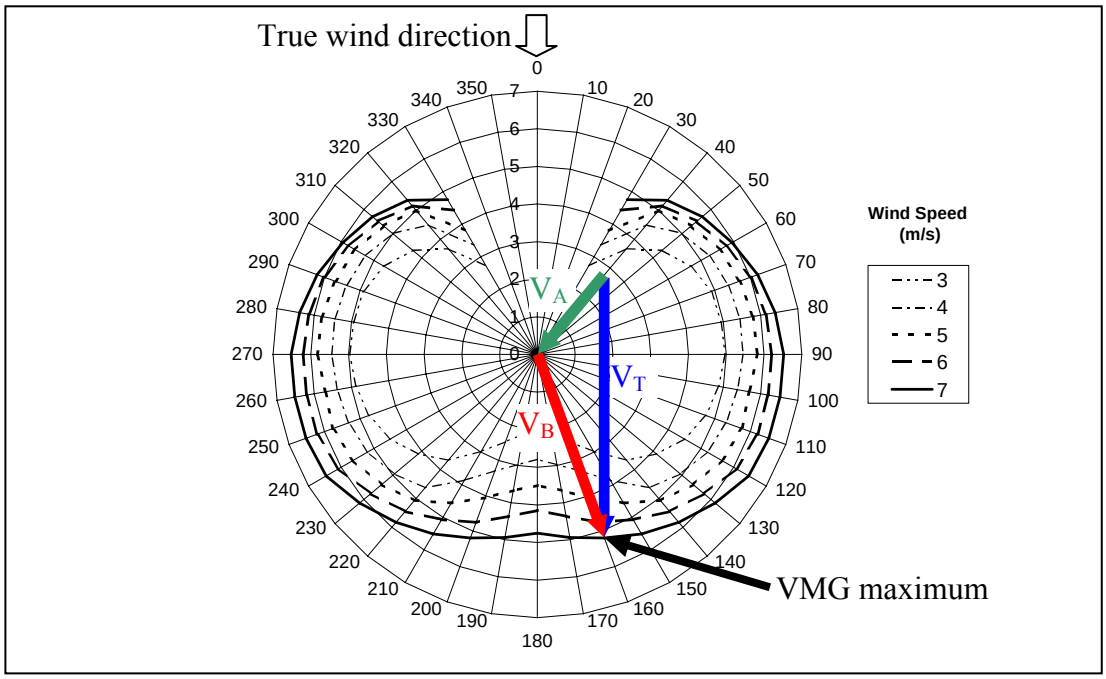


Figure 3: Speed polar for a generic IACC yacht

While the boat speed is the same for all heights on the sails, the true wind speed will vary with height in a manner that can be modelled by a logarithmic boundary layer given by:

$$V_T = \frac{u_*}{\kappa} \ln\left(\frac{z}{z_0}\right) \qquad (2)$$

Where for flows over a water surface the true roughness length is governed by the wave height. Cook [2] gives the over water roughness length as:

$$z_0 \approx 5x10^{-5} \frac{V_T^2}{g} \qquad (3)$$

with $V_T$ the true wind speed at a height of 10m. A true roughness length of 0.25 mm was therefore estimated to be appropriate for these conditions. In both the wind tunnel and the CFD modelling it is the apparent wind that is recreated and this varies in both magnitude and direction with height. Fig. (4) illustrates these vector additions at three heights.

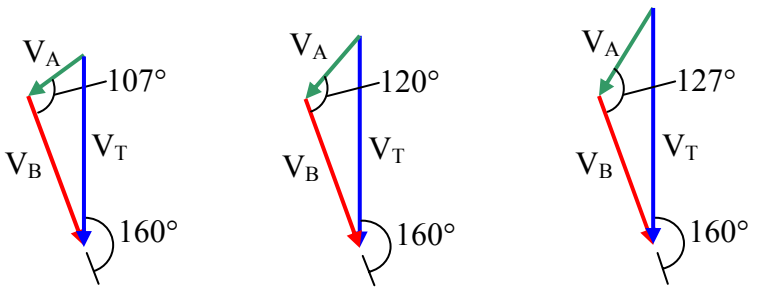


(a) Boom Height z = 3.5 m

(b) Reference Height z = 10 m

(c) Masthead z = 33.9 m

Figure 4: Velocity triangle at three heights; (a) 3.5m, (b) 10m and (c) 33.9m

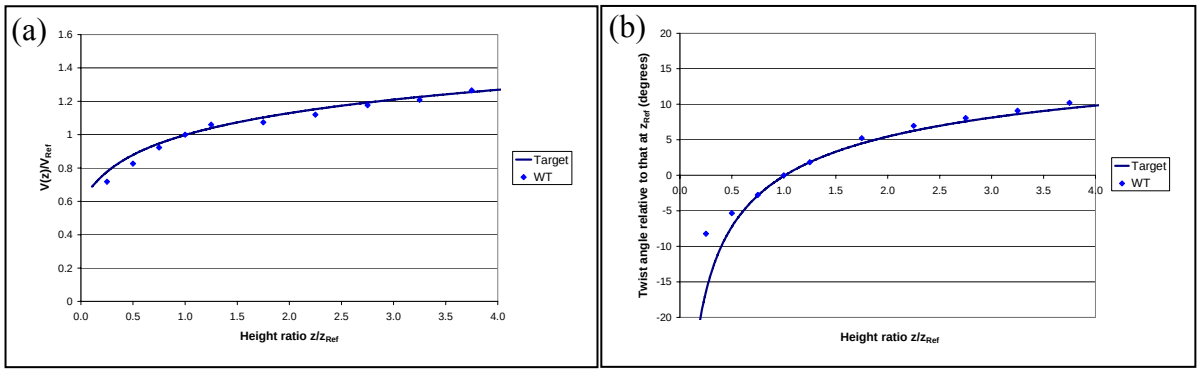


Figure 5: (a) Wind speed and (b) twist profiles

In the wind tunnel various barriers and roughness elements were used to create a wind speed profile similar to the variation in apparent wind speed with height. In addition turning vanes, as seen behind the model in Fig. (1a), were used to provide the appropriate variation of wind direction with height. The model hull is set at the reference apparent wind angle and the vanes adjusted so that the flow is straight at the reference height of 400mm (10m in full-scale) but directs the flow towards the bow of the boat at lower heights and more from the stern at higher levels. The measured wind speed and twist profiles, relative to values at the reference height, are show in Fig. (5). It may be observed that at very low heights the vanes aren't able to create as much twist as suggested by calculation, but since this is generally below the foot of the sails it is of little significance.

The inlet boundary conditions for the CFD model were based on the calculated apparent wind velocity vectors and varied both the wind speed magnitude and direction with height. The corresponding reference dynamic pressure, based on the apparent wind speed at the reference height, is 4.7 Pa. However both the positive pressures predicted on the sails at heights near 10m and the overall forces predicted suggested that the effective reference dynamic pressure was 20% higher and so a reference dynamic pressure of 5.7 Pa has been used in calculating both pressure and force coefficients. Sample computations showed that the predicted stagnation pressures on the sails were sensitive to the inlet dissipation, which is related to the length scale of the turbulence. This suggests that the turbulence model may have difficulty properly converting the relatively large eddies in the atmospheric boundary layer to the small eddies near the stagnation point, and indicates a need for further investigation.

The relative position of the sails was monitored by measuring the angle of the boom (along the foot of the mainsail) and the spinnaker pole (from the mast to the windward lower corner of the spinnaker) to the hull centreline. These angles are illustrated in Fig. (6), where they have been superimposed over a photograph of the wind tunnel model. In order to support the fibreglass sails two spinnaker poles were used but the angle to the windward pole was monitored since this is the only one that would exist with a cloth sail. In some figure legends abbreviations such as P40 M75 are used to indicate a spinnaker Pole angle of 40° and Mainsail boom angle of 75°.

In addition to the pressure measurements, the total forces on the model were measured by a six component force balance located below the floor of the tunnel. Separate windage measurements were made on the model hull and rig, without any sails, and deducted from the total forces. Force estimates for each individual sail were calculated by assigning a contributory area vector to each tap, calculating the associated net force on this area and then summing the components. The total forces obtained by pressure integration were compared to the balance forces, less windage, and as illustrated in Fig. (6b) good agreement is achieved.

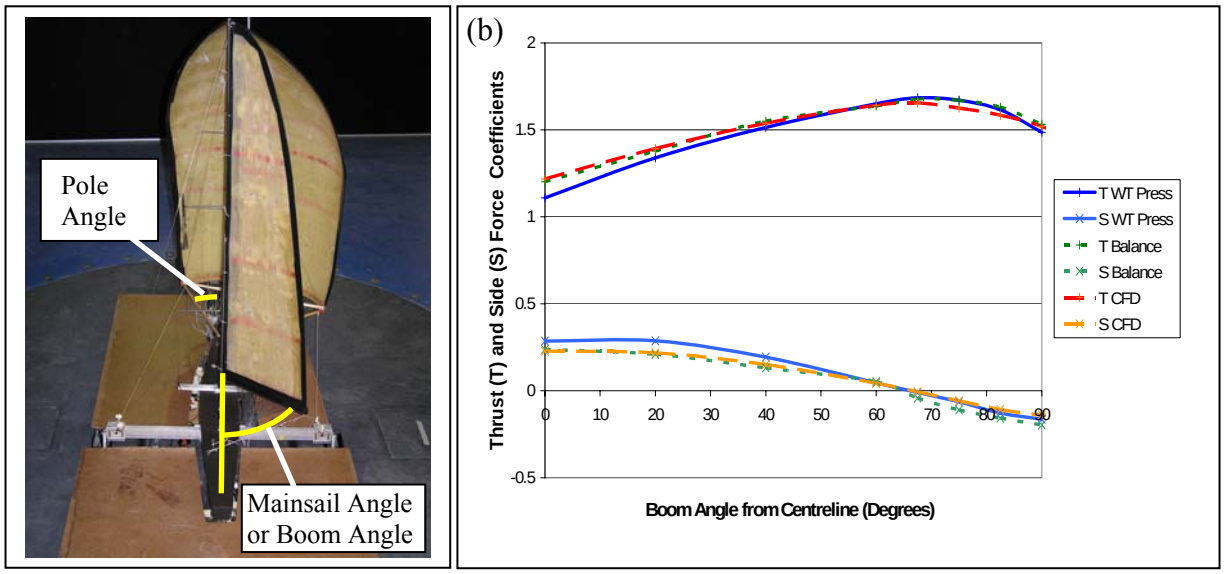


Figure 6: (a) Definition of Mainsail and spinnaker Pole angles, (b) Variation of Trust (T) and Side (S) force coefficients with boom angle for an apparent wind angle of 120° and pole angle of 40°.

In Fig. (6) the force coefficient ($C_F$) is calculate from

$$C_F = \frac{Force}{q_{\text{Ref}} A_{\text{Total}}} \tag{4}$$

where $q_{\text{Ref}}$ is the reference dynamic pressure at the reference height of 10m (full-scale) and $A_{\text{Total}}$ is the total sail area.

The computational modelling made use of the Fluent CFD code [3] in a manner very similar to that described in Ref. [1], except that the problem domain was full scale rather than model scale. The domain was 300 m in width, 87.5 m in height, and 300 m in length. The height of the domain matched the height of the wind tunnel scaled to full size. A doubling of the domain height produced a difference in force coefficients of less than 1.4%, indicating that this height was sufficient to avoid blockage effects.

The CFD domain included the sails, hull and boom, but did not include the mast or rigging. Sample computations were made with a mast included in the model. The differences in lift and drag on the mainsail were less than 3%, and the effect of the mast on the spinnaker forces was negligible. The mast affected the pressure on the front third of the suction side of the main; however, this effect was relatively small. In downwind sailing the main is generally at a high angle of attack and the flow is largely separated, so it is not surprising that the mast does not have a major effect on the results. Due to the added complexity and increased computational time, as well as its relatively minor significance, the mast was not included in the remainder of the computations.

The sails were meshed using tetrahedral cells with an initial grid spacing of 0.7 on the sail surface, increasing at a geometric expansion ratio of 1.08, with a maximum grid spacing of 12.5 m. The convective terms were calculated using a second-order accurate QUICK-type scheme (Leonard and Mokhtari [4]). It was previously shown in [1] that the estimated error in predicted spinnaker force coefficients produced by this grid size was approximately 1.5%. The lift and drag coefficients were monitored in addition to the residuals, and the solution was iterated until either the normalized residuals were less than $2.0 \cdot 10^{-5}$, or the force coefficients changed by less than 0.5% after 100 iterations.

The Realizable *k-ε* model was used for all computations, since Lasher and Sonnenmeier [5] showed that this was the best choice of models available in Fluent for spinnaker flows. Standard wall functions as proposed by Launder and Spalding [6] were used on the surface of the spinnaker as well as the water surface. When using wall functions the distance of the first point from the surface is important. This distance is measured using the variable $y^+ = u_\tau y/\upsilon$, where $u_\tau$ is the shear velocity at the wall $(\tau_{wall}/\rho)^{0.5}$. It is generally recommended that $y^+$ for the first grid points should be no less than 30 but as close to 30 as possible. In the present case most of the first points on the sail surfaces had $y^+$ values between 30 and 200. Lasher and Richards [1] showed that the predicted force coefficients for these flows are not sensitive to either the near-wall grid spacing or the type of wall function used.

In CFD simulations it is possible to model the motion of the water surface relative to the boat, which is not possible in the wind tunnel. The velocity on the inlet, top, and lower surfaces was therefore specified as a vector combination of the true wind speed given in Eq. (2) and the reverse of the boat's motion. The inlet turbulent kinetic energy was set to $3.33u_*^2$ and the inlet turbulent dissipation shown in Eq. (5) was used:

$$\varepsilon = \frac{u_*^3}{\kappa(z+z_o)} \tag{5}$$

The roughness length used in Fluent is defined differently than in Eq. (3); in addition, due to the relative motion of the water surface it was necessary to change $z_o$ so that the shape of the predicted apparent wind velocity profile best matched the actual apparent wind velocity profile. Based on trial and error, $z_o$ was set to a value that minimized the difference between the actual and predicted velocity profiles over a span from the bottom of the main to the top of the mast, which produced a maximum error in velocity magnitude of 1.4%, and a maximum error in apparent wind angle of 0.6°.

Also shown in Fig. (6b) are the force coefficients obtained by integrating the pressures predicted by the CFD modelling. It may be observed that the CFD and Wind Tunnel models exhibit similar variation in the forces with mainsail angle and that any discrepancy is only of the same order as the difference between the integrated pressure and balance values.

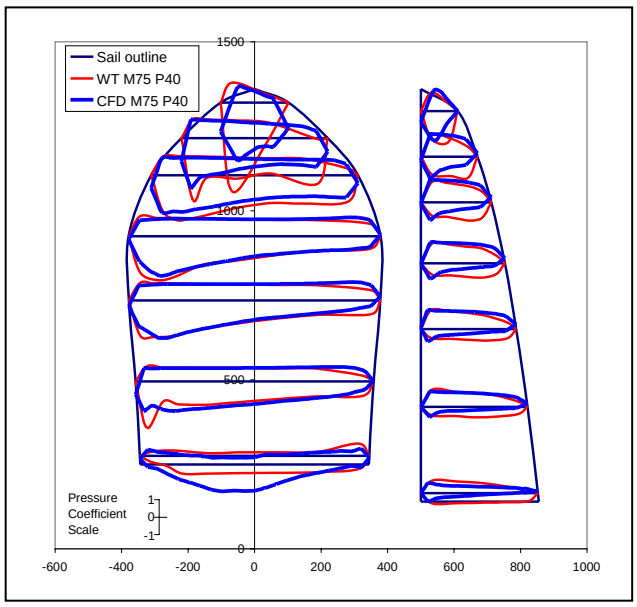


Figure 7: Comparison of the wind tunnel and CFD pressures for a mainsail angle of 75°, pole angle of 40° and apparent wind angle of 120° .

A more detailed comparison of pressures is shown in Fig. (7) for the particular case of mainsail angle 75°, pole angle 40° and apparent wind angle 120°. Fig. (7), and similar figures in this paper, illustrate the pressures at seven levels on each sail. Each horizontal line represents a line of taps and is also the X-axis of each graph, with positive pressures plotted above the line (usually from the windward side of the sail) and negative pressures below the line. The Y axis scale for all 14 sub-graphs is shown in the lower left hand corner, where the pressure coefficient is the ratio of the local pressure to the reference dynamic pressure.

The CFD and wind tunnel pressure distributions in Fig. (7) show general similarities and some differences. These differences are most marked at the head and foot of the sail where the pressure fields show significant localised variations. There is also a general difference between the pressures on the leeward side of the mainsail. It appears that the wind tunnel pressures are more uniform which tends to suggest that the flow is totally separated whereas the CFD distributions, with higher suctions towards the leading edge, suggest a more attached flow. This difference is probably due to the known inability of the turbulence model to accurately predict reattachment of separated flows.

In spite of these detailed differences it does appear that in general both the wind tunnel and CFD model exhibit similar variations in force coefficients as the trim is altered. Hence it is believed that the CFD modelling can be used to provide insight and explanations for the effects seen in the wind tunnel.

## 3 RESULTS AND DISCUSSION

### 3.1 Force contributions from each sail

Preliminary investigations were conducted to find the approximate optimal locations of the spinnaker pole and boom for an apparent wind angle of 120°. The optimum pole angle appeared to be 40°, which with this particular sail means that the sail is positioned symmetrically about the centreline of the yacht. Initial measurements also suggested that the optimum mainsail angle was 75°, since this gave the highest measured thrust force. However later analysis, including corrections for slight variations in dynamic pressure, showed that a slightly lower boom angle, around 67.5°, gave a marginally higher thrust coefficient. Since this analysis wasn't carried out until after the wind tunnel testing was completed, a mainsail angle of 75° was chosen and used as the fixed position when varying pole angles.

During the first systematic series of tests the mainsail angle was varied between 0° and 90° with the pole angle fixed at 40° and the apparent wind angle 120°. The resulting forces obtained by pressure integration, both in the wind tunnel and CFD, are shown in Fig. (8). One of the major advantages of using pressure integration is that the force contributions from each individual sail can be easily determined. Fig. (8) clearly shows that both the wind tunnel and CFD models show similar breakdowns of the thrust and drive forces into the relative contributions from the mainsail and spinnaker. Both sets of results show the maximum thrust occurs with a mainsail angle near 67.5°, at which point about three-quarters of the thrust (WT 75%, CFD 78%) is provided by the spinnaker. At the same time the side forces are very nearly balanced, with the small negative (to windward) side force on the spinnaker balanced by the positive side force on the mainsail.

Fig. (8) shows that the mainsail angle has only a small effect on the spinnaker, with both the thrust and side force relatively constant. At the same time changing the angle of the mainsail has obvious effects on the mainsail forces. This is partially due to the geometric changes whereby at 0° the sail is principally parallel to the centreline and hence contributes little to the thrust, whereas at 90° any pressure difference across the sail will drive the yacht forward.

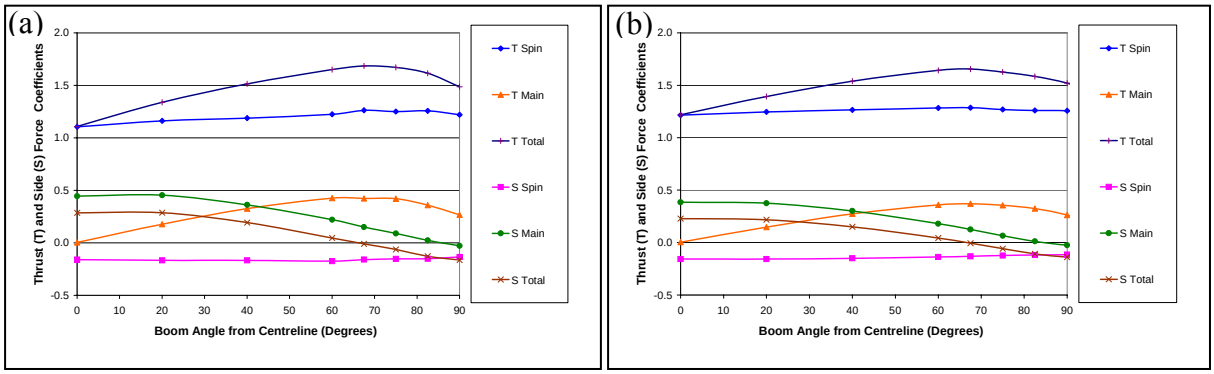


Figure 8: The effects of varying boom angle when the spinnaker pole is at 40° and the apparent wind angle 120°. Thrust and side forces on each sail as calculated by pressure integration. (a) Wind tunnel and (b) CFD.

However there are also major changes in the character of the flow around the sails. Fig. (9a) shows the lift and drag force coefficients for the mainsail as a function of the boom angle. Both the wind tunnel and CFD results show the highest mainsail drag occurs with the boom at about 30° to the centreline, which is to be expected since at this angle the sail is perpendicular to the apparent wind. The maximum lift occurs at about 80°, which corresponds to an angle of attack of 40°. This is quite a high angle for maximum lift, but is not surprising since the mainsail aspect ratio is only about 4.5 and so the sail is strongly affected by downwash. Although the mainsail changes from creating drag to lift as the mainsail is eased, as shown by Fig. (9b), the pressure distributions remain quite similar. With the boom at 0° the suction pressures on the leeward side of the mainsail are quite uniform, whereas at 75° there is a definite shift in the maximum suction towards the luff, but this is the only significant change. These changes in distribution are consistent with the CFD flow visualisations shown in Fig. (10).

Fig. (10) shows the streamlines, released at a height about half way up the sails, for mainsail boom angles of 0°, 40°, 60° and 75°. The viewing point for these images is such that the windward side of the mainsail is visible. The black line along the foot of the red mainsail indicates the position of the boom. These images clearly show that with the boom at 0° the flow is completely separated, but as the sail is eased the size of the separation zone is reduced and at 75° the flow appears to remain attached to the leeward surface of the mainsail.

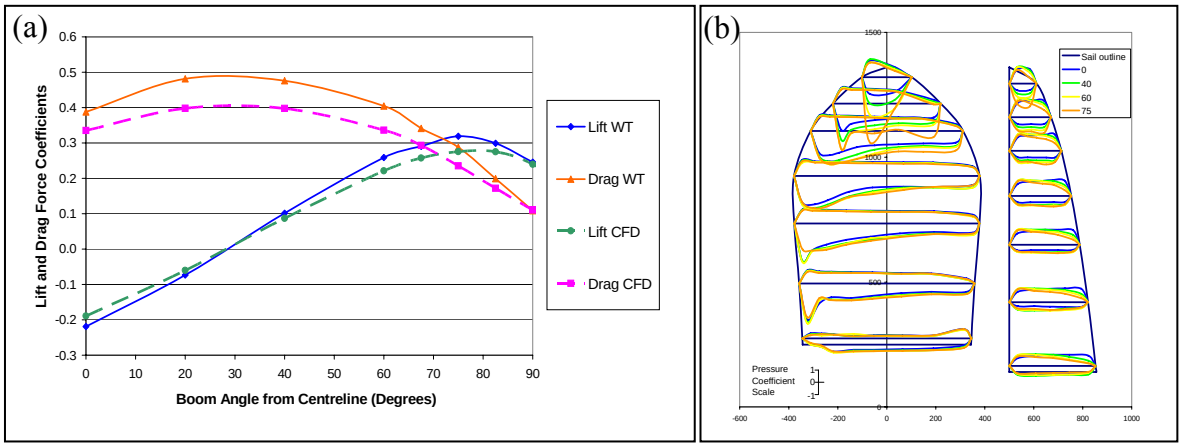


Figure 9: (a) Lift and drag force coefficients for the mainsail with varying boom angle from both the wind tunnel and CFD and (b) Wind tunnel pressure distributions for selected boom angles. The spinnaker pole is at 40° and the apparent wind angle 120°.

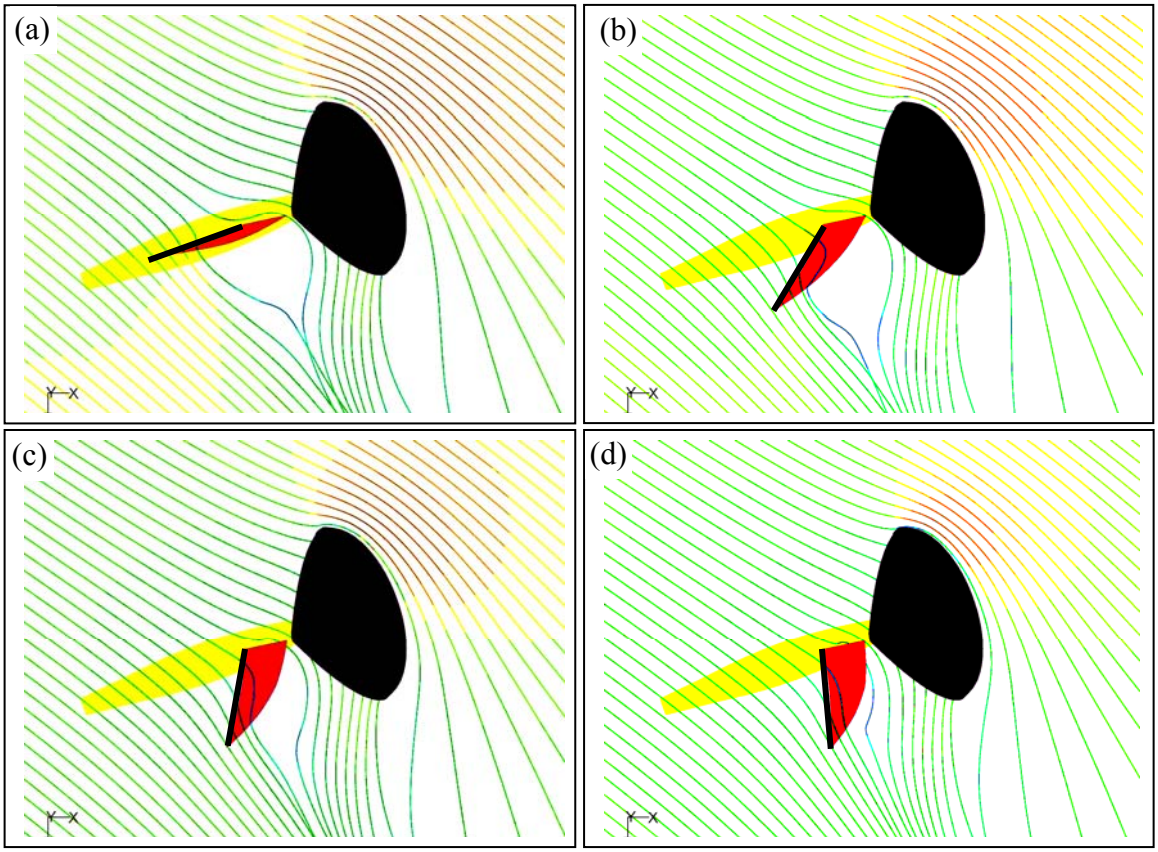


Figure 10: CFD streamlines released from a height of 18.375 m (full-scale) for four boom angles (a)0°, (b) 40°, (c) 60° and (d)75°. The spinnaker pole was at 40° and the apparent wind angle 120°.

### 3.2 Constructive interactions

In order to investigate the interaction between the sails, wind tunnel measurements and CFD simulations were also made with each sail on its own. Fig. (11) is similar to Fig. (8) but also includes the data from the single sail tests (dashed lines). These single sail forces have also been combined to give a "summed" total force, which shows what force might be obtained if there was no sail interaction. Both sets of results show that the strongest destructive interaction occurs when the boom angle is greater than 75°, and so this will be the subject of the next section. The wind tunnel results show that for boom angles less than 75° the forces on the mainsail are not significantly modified by the presence of the spinnaker, however it does appear that the mainsail has a beneficial effect on the spinnaker. The CFD data is slightly different in that it shows a slight reduction in both the thrust and side force on the mainsail for boom angles less than 75°, but does show similar increases in the spinnaker forces with the mainsail present. Both sets of results show that the maximum thrust obtained from the sails together is slightly higher than the "summed" values from the individual tests. Hence it appears that at the best trim the sail interaction is beneficial.

Some aspects to this interaction are visible in the streamlines of Fig. (10). As the main is eased from 0 to 75°, the streamlines on the suction side of the spinnaker more closely follow the contour of the spinnaker, consistent with a decrease in pressure on the suction side of the spinnaker shown in the pressure plots of Fig. (9b). There is also a perceptible difference in the upwash near the leading edge of the spinnaker. Both of these effects indicate an increase in circulation around the spinnaker, which is reflected in the increase in forces.

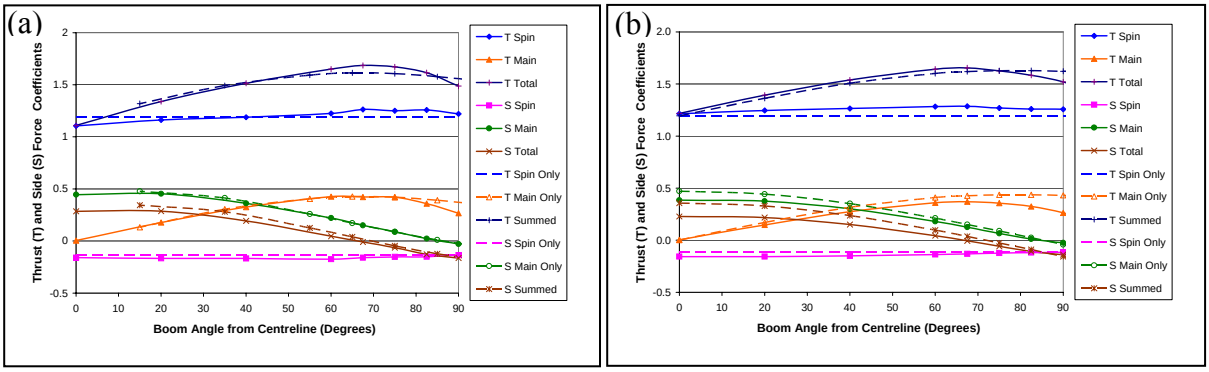


Figure 11: The effects of varying boom angle when the spinnaker pole is at 40° and the apparent wind angle 120°. Thrust and side forces from tests with both sails (solid lines) and from single sail tests (dotted lines). (a) Wind tunnel and (b) CFD.

Figs. (12a) and (12b) show the streamlines with the spinnaker pole at 40° with and without the mainsail (at 75°). The streamlines are coloured by velocity (red being the highest). The figure with the main shows a slightly larger red area near the leading edge of the spinnaker on the suction side, indicating higher velocities. The streamlines are also visibly more deflected near the trailing edge of the spinnaker when the main is present.

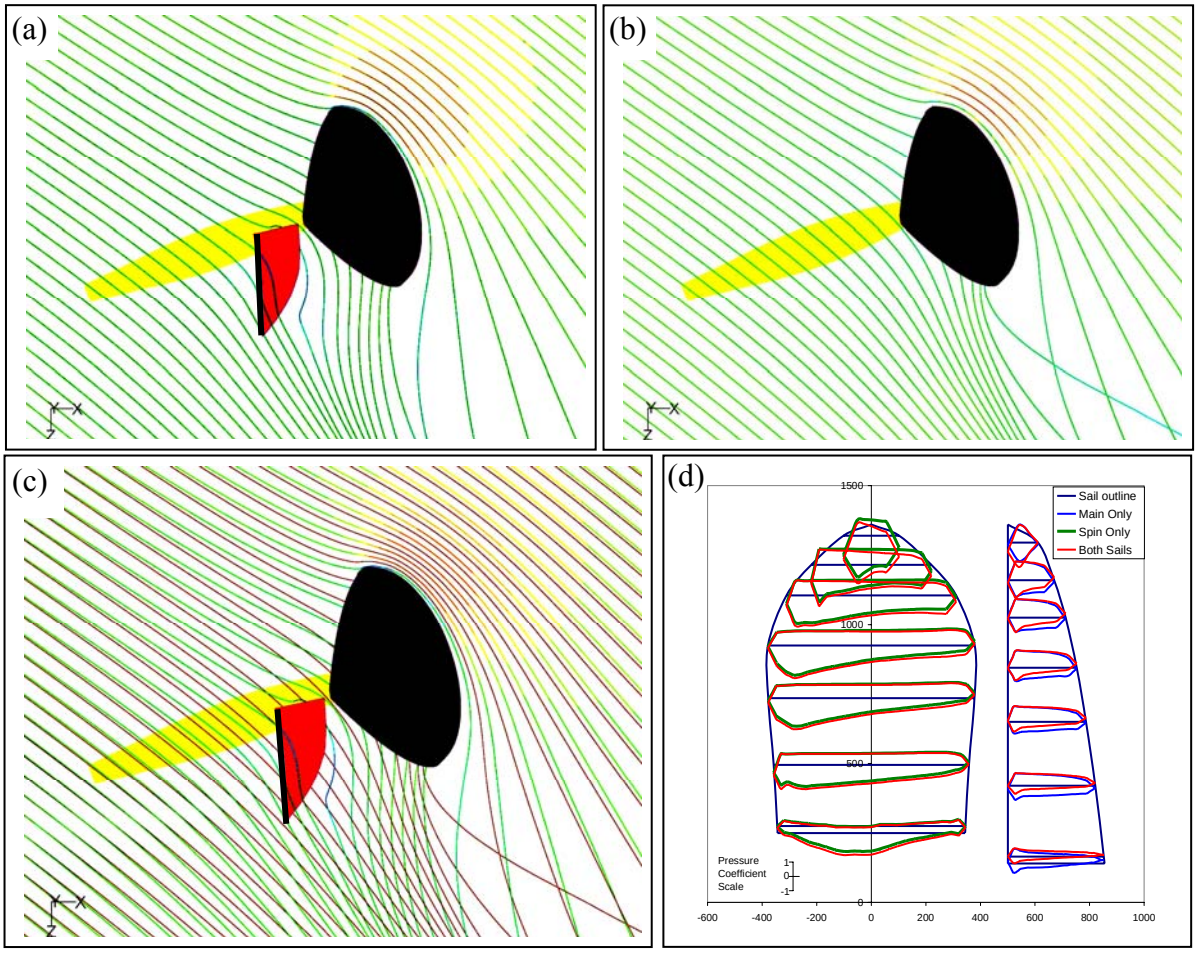


Figure 12: CFD streamlines released from a height of 18.375 m (full-scale) when the spinnaker pole was at 40° and the apparent wind angle 120°, (a) with the mainsail boom at 75°, (b) without the mainsail, (c) with the two sets of streamlines superimposed and (d) the CFD pressures for the two sails tested together and alone.

Fig. (12c) shows the streamlines for the no-main case (in red) superimposed over the case with the main. There is significant increase in the upwash near the leading edge of the spinnaker when the main is included, as shown by the larger deflection of the green streamlines compared to the red streamlines. This and the increased deflection of the streamlines near the trailing edge show that the presence of the main increases the circulation around the spinnaker, which results in higher velocities and lower pressures on the suction side.

Fig. (12d) shows the corresponding pressures from the CFD simulations. These show that when the mainsail is present the suction pressures on the leeward side of the spinnaker are generally increased, thus leading to higher thrust forces. However the suction pressures on the leeward side of the mainsail are decreased resulting in less thrust from the mainsail as seen in Fig. (11b).

### 3.2 Destructive interactions

The destructive interaction between the spinnaker and mainsail becomes even stronger if the boom angle is increased beyond 75°, resulting in a reductions in both the mainsail thrust and the total thrust. This destructive effect is even more apparent with lower apparent wind angles, where the spinnaker pole angle for maximum thrust is reduced. Fig. (13a) shows the wind tunnel force data for an apparent wind angle of 120° and the corresponding pole angle of 40°, previously shown in Fig. (11a), together with a second series where the apparent wind angle was reduced to 100° and the pole angle reduced to 20°. The velocity and twist profiles used were the same for the two series of tests. The results show that since the angle of the wind relative to the spinnaker remains the same the forces on the spinnaker are very similar. However since the position of the hull relative to the spinnaker has changed, the components of the spinnaker forces are modified resulting in the spinnaker side force changing sign. A more significant change is apparent for the mainsail. This occurs as a result of the leech (trailing edge) of the spinnaker moving aft and hence the interaction between the mainsail and spinnaker becomes important at lower boom angles. The overall effect of this interaction is to slightly reduce the maximum total drive force that can be achieved (from $C_T$ =1.69 to 1.56) and to modify the boom angle at which this occurs (from 67.5° to approximately 50°).

Fig. (13b) shows the lift and drag forces on the mainsail for the interacting sails and for the mainsail alone. It is clear that at small boom angles, high angles of attack, there is little effect of the spinnaker on the mainsail but at higher boom angles, lower angles of attack, the presence of the spinnaker reduces both the mainsail lift an drag, with the major effect being a reduction in lift.

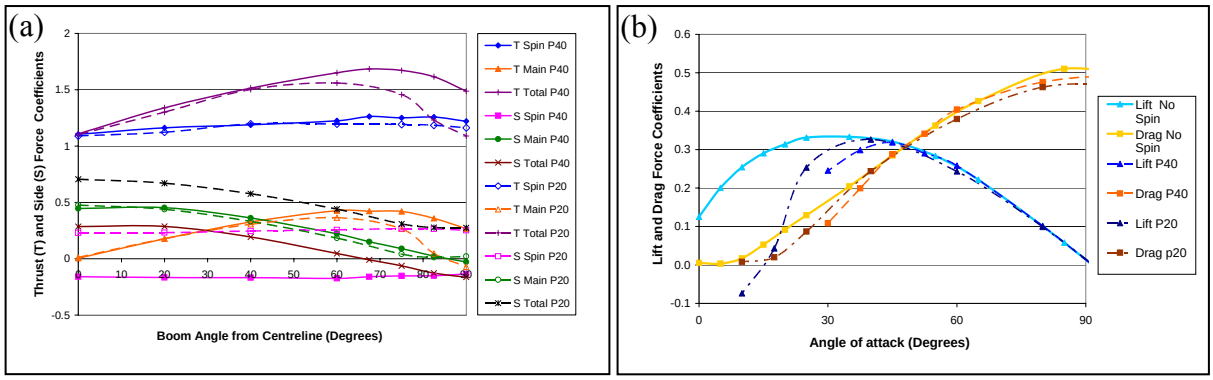


Figure 13: (a) Wind tunnel forces for spinnaker pole/apparent wind angle combinations of 40°/120° (solid lines) and 20°/100° (dashed lines), (b) The corresponding mainsail lift and drag force coefficients in relation to the mainsail angle of attack (apparent wind angle – boom angle) together with the no spinnaker data.

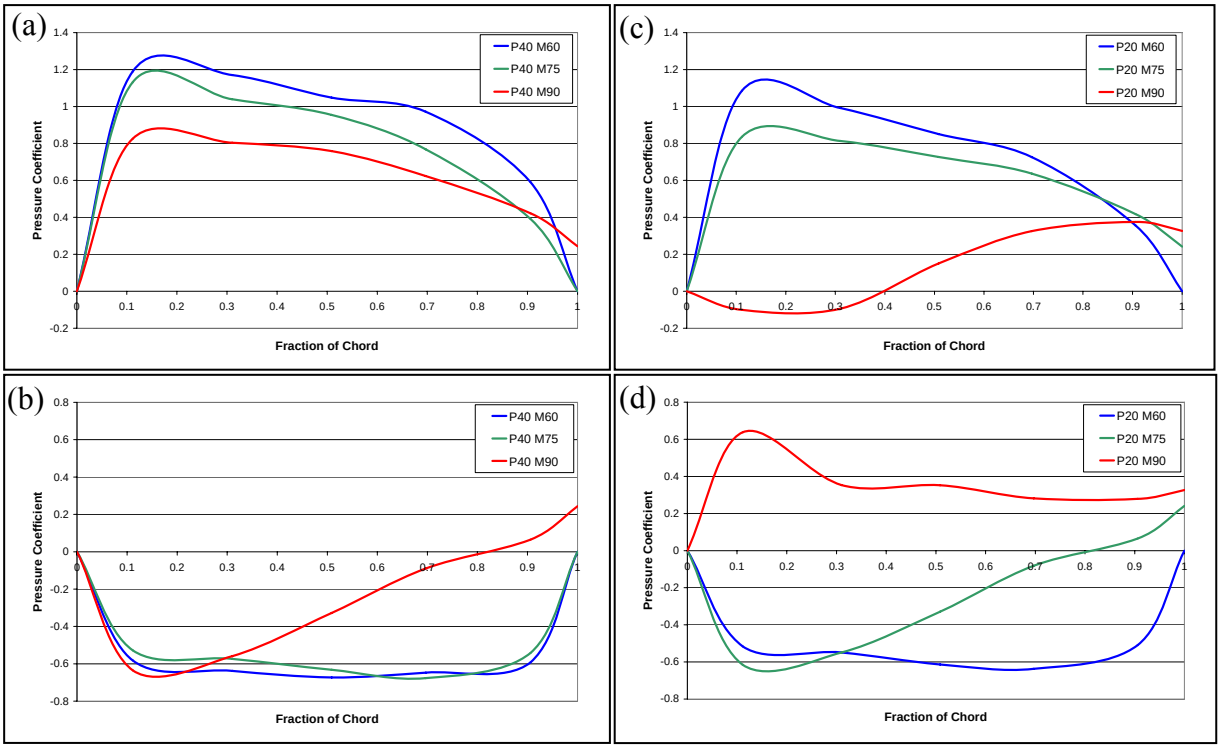


Figure 14: The effects of boom angle on wind tunnel mainsail pressure distributions at a height of 650 mm when the spinnaker pole is at 40° and the apparent wind angle 120°: (a) windward and (b) leeward, together with those for a spinnaker pole angle of 20° and apparent wind angle of 100°: (c) windward and (d) leeward.

Fig. (14) illustrates the mainsail pressure distribution at about mid-mast. With the pole angle at 40°, Figs. (14a and b), increasing the boom angle from 60° to 75° simply reduces the positive pressures on the windward side of the sail, which is a result of the reduction in angle of attack (from 60° to 45°). However as the boom moves from 75° to 90° there is marked change in the pressures on the leeward side of the sail, possibly indicating flow reattachment. With the spinnaker pole further forward (20°) and a lower apparent wind angle (100°) the pressure distributions when the boom angles are 60° and 75° are very similar to those obtained at angles of 75° and 90° when the apparent wind was further aft, which is to be expected since the angles of attack are similar. However when the boom is let out to 90° the differential pressure on the windward half of the mainsail changes sign and would result in a cloth sail inverting. This is observed to occur even thought the angle of attack is still 10°. Both this observation and the data in Fig. (13b) suggest that the spinnaker has effectively changed the direction of the flow affecting the mainsail and hence the effective angle of attack is markedly smaller than that obtained from the geometry. This concept is also supported by the streamlines in Fig. (12b), where the spinnaker is observed to have changed the flow direction in the region where the mainsail is normally located. While a change in angle of attack partially explains the effect of the spinnaker on the mainsail it does not appear to be a complete explanation, since the pressures on both sides of the trailing edge of the mainsail become progressively more positive as the boom angle is increased. This phenomenon may be more associated with the positive pressures generated on the windward side of the spinnaker overlapping and influencing the pressures around the mainsail when they are in close proximity.

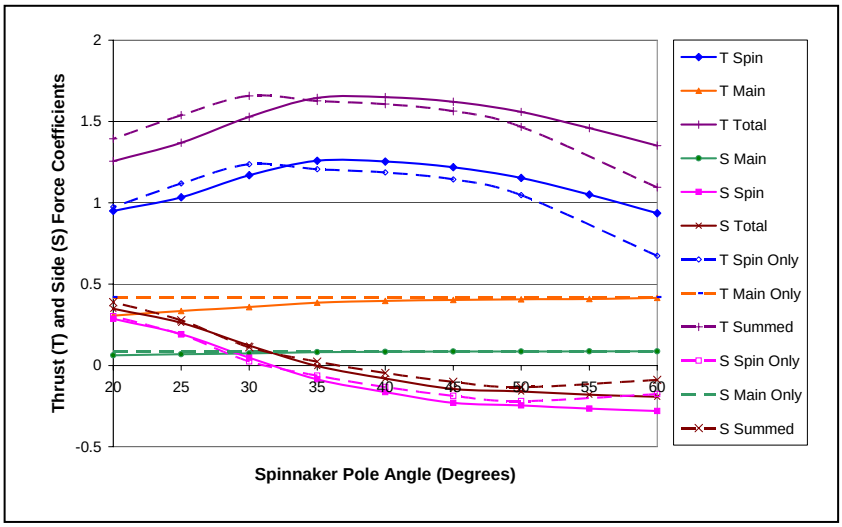


Figure 15: The effects of varying spinnaker pole angle when the boom is at 75° and the apparent wind angle 120°. Thrust and side forces on each sail as calculated by pressure integration from tests with the two sails together (solid lines) and independently (dashed lines).

### 3.3 Spinnaker pole angle variation

Fig. (15) shows the results from a series of tests where the boom was at 75° and the spinnaker pole angle varied. These show that the highest thrust force is obtained with the pole angle around 40°. At lower pole angles the proximity of the spinnaker reduces the suction on the leeward side of the main, as illustrated in Fig. (16), and the suction on the leeward side of the spinnaker become very uniform, which indicates that the flow is separated. On the other hand with the pole further aft, higher angles, the pressures near the leeward leading edge (luff) of the spinnaker change sign. In practice this leads to the luff curling under and partially collapsing. At intermediate angles there are strong suctions pressures over much of the leeward side of the spinnaker leading to the high thrust forces.

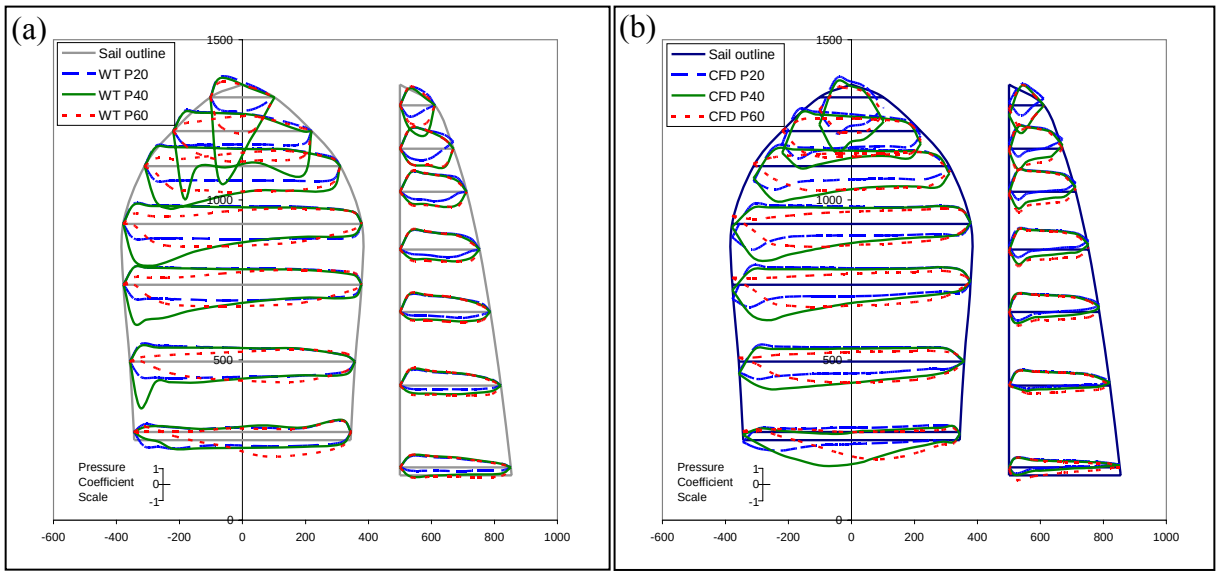


Figure 16: Pressures on the mainsail and spinnaker for three spinnaker pole angles (20, 40 and 60°) obtain from (a) wind tunnel testing and (b) CFD modelling. The boom was at 75° and the apparent wind angle 120°.

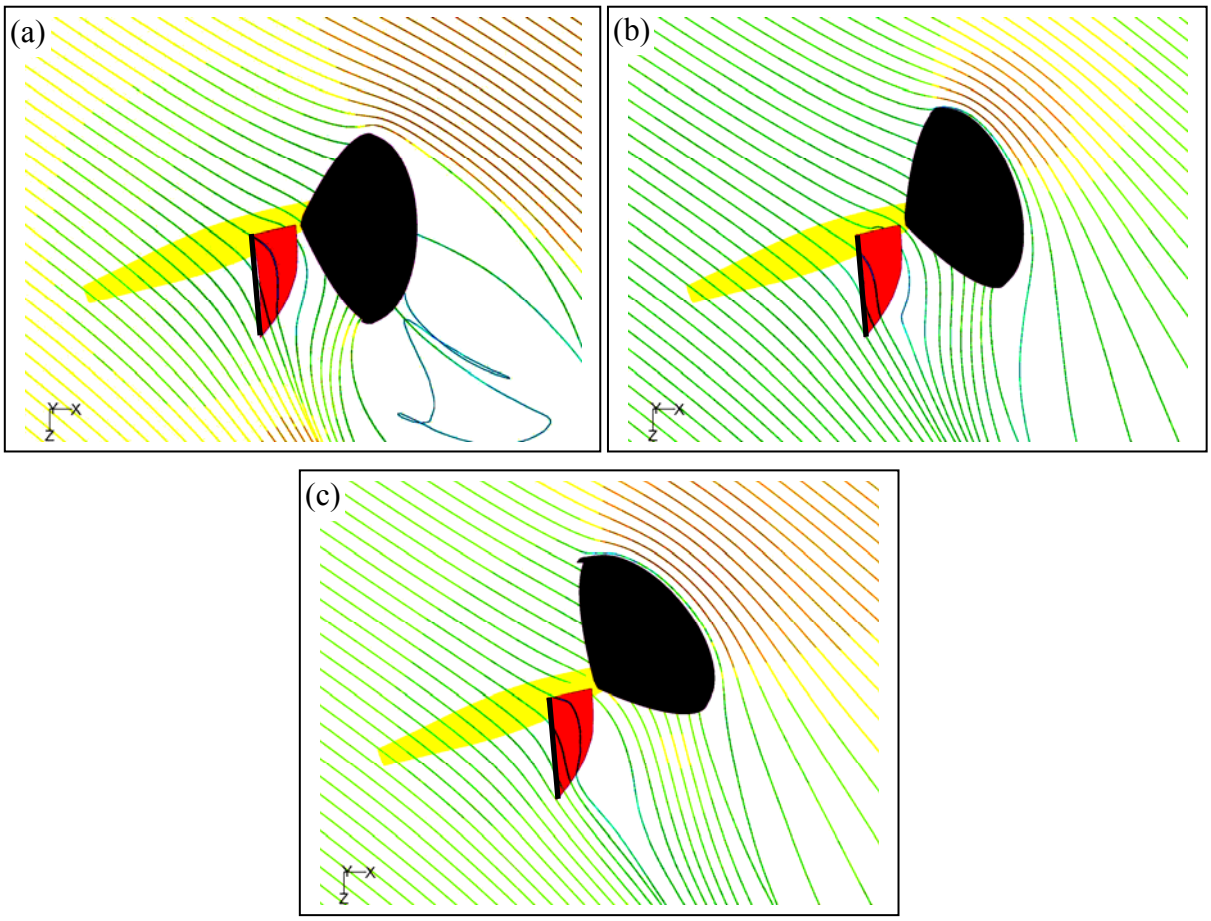


Figure 17: CFD streamlines released from a height of 18.375 m (full-scale) when the boom was at 75° and the apparent wind angle 120°, (a) with the spinnaker pole at 20°, (b) 40° and (c) 60°.

These flow patterns are illustrated by the CFD generated streamlines of Fig. (17). With the spinnaker pole at 20° the flow around the spinnaker is clearly separated, and the deflection of the air into the mainsail is at a maximum. At 40° the flow around the spinnaker is mostly attached and there is an increase in the upwash near the leading edge of the spinnaker and a decrease in the redirection of the flow towards the main. This results in an increase in circulation and thus an increase in lift. When the pole is pulled back to 60° the upwash near the leading edge of the spinnaker decreases, and there is less deflection of the streamlines near the trailing edge. This results in a decrease in circulation and drop in forces on the spinnaker. In addition with the higher pole angle the flow is stagnating on the outside of the spinnaker luff and would therefore cause the sail to collapse.

Also shown in Fig. (15) are the forces obtained from the individual sails. These comparisons reinforce the idea that having the spinnaker and mainsail in close proximity, as occurs when the pole is at 20°, decreases the suction pressures on the leeward side of the mainsail and hence reduces the mainsail thrust. In addition it appears that the presence of the mainsail alters the flow onto the spinnaker by about 5°. It can be observed that the general shape of the spinnaker thrust–pole angle curve is similar with and without the mainsail, but is shifted to slightly higher pole angles when the mainsail is present. This is consistent with the enhance upwash observed in Fig. (12c).

## 4 CONCLUSIONS

Wind tunnel testing of pressure tapped fibreglass downwind sails and CFD modelling have been used to investigate the flow around and the interactions between a 1/25$^{th}$ scale IACC spinnaker and mainsail. It has been shown that when trimmed for maximum thrust the mainsail has a small beneficial effect on the flow around the spinnaker. However at the same time the spinnaker has a small adverse effect on the mainsail. This adverse effect is more significant if the mainsail is let out too far and is also more apparent at lower apparent wind angles when the spinnaker pole is well forward and the spinnaker trailing edge further aft. These interaction effects have been shown to be a mixture of changes to the local flow angles and the overlapping of the pressure fields around each sail.

## REFERENCES

[1] W. Lasher, P.J. Richards. Validation of RANS simulations for spinnaker force coefficients in an atmospheric boundary layer. *Journal of Ship Research*, 51(1), 22-38, 2007.

[2] N.J. Cook. The designer's guide to wind loading of building structures, Part 1, *Butterworth*, 1985.

[3] Fluent. Fluent 6.3 User's Guide, Fluent, Inc., Lebanon, NH, 2006.

[4] B.P. Leonard, S. Mokhtari. ULTRA-SHARP Non-oscillatory Convection Schemes for High-Speed Steady Multidimensional Flow, NASA TM 1-2568 (ICOMP-90-12), NASA Lewis Research Center, 1990.

[5] W.C. Lasher, J.R. Sonnenmeier. A practical analysis of RANS simulations for spinnaker aerodynamics, Journal of Wind Engineering and Industrial Aerodynamics, vol. 96, no. 2, pp. 143-165, February 2008.

[6] B.E. Launder, D.B. Spalding. The Numerical Computation of Turbulent Flows, Computer Methods in Applied Mechanics and Engineering, 3, 269-289, 1974.